JOURNAL OF SYNCHROTRON RADIATION
ISSN 1600-5775

Received 2 March 2020
Accepted 14 August 2020

Edited by S. M. Heald, Argonne National Laboratory, USA

Keywords: X-ray absorption fine structure; bent crystal Laue analyser; total reflection fluorescence X-ray absorption fine structure; *in situ* surface X-ray absorption fine structure.

Supporting information: this article has supporting information at journals.iucr.org/s

Bent crystal Laue analyser combined with total reflection fluorescence X-ray absorption fine structure (BCLA + TRF-XAFS) and its application to surface studies

Yuki Wakisaka,[a] Bing Hu,[a] Daiki Kido,[a] Md. Harun Al Rashid,[a] Wenhan Chen,[a] Kaiyue Dong,[a] Takahiro Wada,[b] Bapurao Bharate,[a] Quiyi Yuan,[a] Shingo Mukai,[a] Yasuo Takeichi,[c] Satoru Takakusagi[a] and Kiyotaka Asakura[a]*

[a]Institute for Catalysis, Hokkaido University, Kita 21-10, Sapporo, Hokkaido 001-0021, Japan, [b]Tokyo Medical and Dental University, Yushima, Bunkyo-ku, Tokyo 113-8549, Japan, and [c]Institute for Materials Structure Science, High Energy Accelerator Research Organization, Oho 1-1, Tsukuba 305-0801, Japan.
*Correspondence e-mail: askr@cat.hokudai.ac.jp

A bent crystal Laue analyser (BCLA) is an X-ray energy analyser used for fluorescence X-ray absorption fine-structure (XAFS) spectroscopy to separate the fluorescence X-ray emission line of a target atom from the elastic scattering X-rays and other fluorescence emission lines. Here, the feasibility of the BCLA for total reflection fluorescence XAFS (TRF-XAFS), which has a long X-ray footprint on the substrate surface owing to grazing incidence, was tested. The focal line of the BCLA was adjusted on the X-ray footprint and the XAFS signal for one monolayer of Pt deposited on a 60 nm Au film with high sensitivity was obtained. Although range-extended XAFS was expected by the rejection of Au fluorescence arising from the Au substrate, a small glitch was found in the Au L_3 edge because of the sudden change of the complex refraction index of the Au substrate at the Au edge. This abnormal spectrum feature can be removed by reflectivity correction using Au foil absorption data. BCLA combined with TRF-XAFS spectroscopy (BCLA + TRF-XAFS) is a new technique for the *in situ* surface analysis of highly dispersed systems even in the presence of a liquid overlayer.

1. Introduction

Polarization-dependent total reflection fluorescence X-ray absorption fine-structure (PTRF-XAFS) spectroscopy is a powerful technique used to determine the three-dimensional structures of metal atoms (10^{13}–10^{15} cm^{-2}) dispersed on single-crystal surfaces. The PTRF-XAFS method requires a flat surface to attain total reflection. Under total reflection conditions, X-rays can penetrate a few nanometres into the solid. Thus, the method is surface-sensitive in spite of the large penetration power of X-rays. X-rays can pass through the gas phase, and thus *in situ* PTRF-XAFS measurements can be performed in the presence of a gas phase (Tanizawa *et al.*, 2003; Chun *et al.*, 1997; Asakura *et al.*, 1997). In addition, the PTRF-XAFS method can be applied to surface analysis in the liquid phase (Masuda *et al.*, 2012; Yuan *et al.*, 2018, 2017; Gullikson, 2001; Henke *et al.*, 1993; Nelson *et al.*, 1994). However, the elastic X-ray scattering of the liquid overlayer becomes large and causes a serious increase of background X-rays; hence the liquid overlayer should be made as thin as possible. Such a very thin liquid overlayer hinders solute diffusion, which is necessary to follow the structural changes of the surface species under a steady-state reaction or to

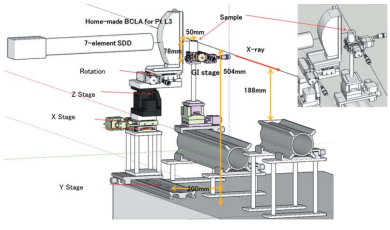

observe the transient states in potential jump experiments (Yamakata *et al.*, 2006). On the other hand, crystal monochromators can be used to reduce scattering from solution (Sa, 2014). The bent crystal Laue analyser (BCLA) is a portable and simple version of a crystal monochromator which can distinguish scattering and fluorescence of X-rays by their energies (Sakayanagi, 1982; Zhong *et al.*, 1999; Kropf *et al.*, 2003; Kujala *et al.*, 2011; Karanfil *et al.*, 2012). The angle between the log-spiral surface and a radial line from one point (called a focal point) is constant along the log spirally bent surface. When the angle is equal to the Bragg condition, all of the X-rays with a constant wavelength are diffracted (Sakayanagi, 1982). We previously measured the X-ray absorption fine structure (XAFS) of one monolayer (ML) of Pt on thin highly oriented pyrolytic graphite (HOPG) using the BCLA combined with the back-illuminated (BI)-XAFS method (Uehara *et al.*, 2014; Asakura, 2016; Wakisaka *et al.*, 2019, 2018; Takahashi *et al.*, 2019).

We found that the following conditions must be satisfied to reduce the background and to obtain a stronger signal using the BCLA:

(1) *A small focal point.* The focus size must be less than 100 µm in the energy dispersion direction (Uehara *et al.*, 2014; Asakura, 2016). The use of a third-generation synchrotron radiation source with emittance less than 10 nm rad is mandatory to obtain a signal from an ML metal film on a substrate. Actually the BCLA provides only the XANES (X-ray absorption near-edge structure) region at the Photon Factory (PF), which has an emittance of 34 nm rad, although at SPring-8 (emittance = 2.4 nm rad) provided the extended XAFS (EXAFS) oscillation appearing at more than 50 eV for the same sample by the same method.

(2) *An accurately bent crystal.* In a commercial BCLA, the crystal is only bent by log-spiral-shaped side frames on which the edges of the thin Si crystal are fixed. The middle of the crystal is open and free. In order to more accurately bend the Si(111) crystal along the log-spiral curve, we constructed a new type of BCLA (Fig. S1 of the supporting information) (Wakisaka *et al.*, 2019). This BCLA has multiple beams to support the crystal in a log-spiral curve. The outer beam positions and directions are consistent with the slits behind the crystal. The positions of the inner beams agree with those of the outer beams and their directions are pointed to the focus.

(3) *Fine adjustment of the BCLA position.* The focal point of the BCLA should agree with the X-ray irradiated point on the sample to effectively collect the fluorescence X-rays. The beam size on the sample must be on the order of 100 µm in the energy-dispersion direction. The adjustment stage should have xz freedom with such resolutions.

After improvement of these three points we successfully removed X-ray elastic scattering from solution and obtained XAFS spectra of 1 ML of Pt on thin HOPG using BCLA + BI-XAFS (Takahashi *et al.*, 2019; Wakisaka *et al.*, 2019; Feiten *et al.*, 2020).

The BCLA removes the scattering X-rays from the sample so that the combination of BCLA and PTRF-XAFS is more promising for the *in situ* measurement of the solid–liquid interface system. The problem that hinders the application of the BCLA for PTRF-XAFS measurement is condition (1) discussed above, which is a necessity for a point focus X-ray less than 100 µm while the total reflection condition provides a footprint longer than 10 mm on the sample surface. However, considering the principle of the BCLA, a small size is only necessary in the vertical-dispersion direction. The Bragg condition is satisfied on the intersectional curve of the BCLA crystal surface and the plane created by the surface normal vector (**n**), radial vector (**r**) and focal point, as shown in Fig. S2. The focal points of the other parts of the curved crystal surface create a focal line. If the long footprint of the incidence X-ray on the surface and the BCLA focal line are adjusted to be in agreement, all of the emitted fluorescence from the X-ray footprint can be used (Fig. S2). Although exact adjustment of the X-ray footprint and focal line is challenging, it improves the fluorescence signal and reduces background scattered X-rays.

In this paper, we investigate the feasibility of BCLA combined with total reflection fluorescence XAFS (BCLA + TRF-XAFS) spectroscopy by applying to 1 ML of Pt deposited on polycrystalline Au in *s*-polarization. First we discuss the feasibilities of the combination of the BCLA and TRF-XAFS. Second, we discuss the possibility of range-extended TRF-XAFS by BCLA. We expected range-extended XAFS of Pt on the Au substrate using the BCLA, which would remove the Au $L\alpha$ fluorescence signal above the Au L_3 edge (Glatzel *et al.*, 2009; Yano *et al.*, 2005; Wakisaka *et al.*, 2018; Asakura *et al.*, 2018; Takahashi *et al.*, 2019). Finally, we showed the preliminary result of the BCLA and TRF-XAFS in the presence of a 1 mm-thick overlayer solution under the applied potential.

2. Experimental

A thin Pt layer was deposited on a 60 nm-thick polycrystalline Au thin film evaporated on a 10 mm × 20 mm Si(100) wafer by self-terminating electrodeposition (Liu *et al.*, 2012, 2015). Pt was electrochemically deposited on an Au polycrystal from 3 mmol K_2PtCl_4–NaCl at pH 4 with an applied voltage of −0.7 V versus Ag/AgCl. The deposition time was 20 s. Hereafter, the sample is called Pt/Au/Si. The Pt coverage was estimated to be 1 ML thick by X-ray photoelectron spectroscopy (XPS). The XAFS measurements were carried out at beamline BL-15A1 of the Photon Factory (PF) in the Institute of Materials Structure Science, High Energy Accelerator Research Organization (Igarashi *et al.*, 2016). The PF storage ring was operated at 2.5 GeV and 450 mA. The X-rays emitted from the short-gap undulator at beamline BL-15A1 were monochromated by an Si(111) double-crystal monochromator. A bent mirror was used to vertically focus the beam. The spot size was 0.1 mm in the vertical direction. The X-ray intensity was monitored by an I_0 ionization chamber filled with N_2. The fluorescence signal was detected by a seven-element silicon drift detector (SDD) (Techno-AP, Tsukuba, Japan), as shown in Fig. 1. The Pt/Au/Si sample was set in front of the SDD. A home-made BCLA was placed between the

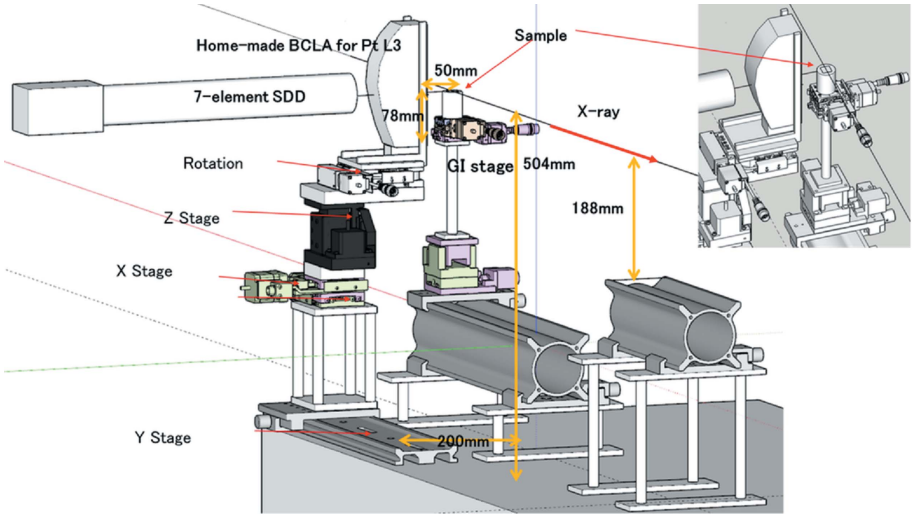

Figure 1
Schematic of the TRF-XAFS system. The incident X-rays come from the left side and the fluorescent X-rays are analysed by BCLA. The BCLA is covered with a lead sheet, except for its entrance and exit windows.

SDD and the Pt/Au/Si sample (Uehara *et al.*, 2014; Wakisaka *et al.*, 2019). The BCLA parameters are described in Section S1 of the supporting information. The energy resolution of the home-made BCLA was estimated at 30 eV judging from the *z*-scan of the Pt $L\alpha_1$ peak full width at half-maximum (FWHM).

We measured Pt/Au/Si under ambient conditions. The initial total reflection conditions were adjusted by a goniometer under the sample without the BCLA. The incident X-ray angle against the sample was set to 4.5 ± 1.0 mrad. The BCLA was then set and adjusted in the *z* direction (dispersion direction) and *x* direction (distance between the sample and the BCLA) by monitoring the Pt L_3 fluorescence signal. We then adjusted ω (parallelism between the X-ray footprint and crystal surface, as shown in Fig. S2) together with *x* and *z* to obtain the maximum fluorescence.

In order to examine the possibility of *in situ* TRF-XAFS measurements, we prepared a 0.1 ML of Pt on Au(111) by spontaneous deposition of $PtCl_6^{2-}$ by dipping the Au(111) surface in 0.1 ml $HClO_4$ + 1 m*M* H_2PtCl_6 for 30 s. This sample was prepared in order to demonstrate the surface species on Au(111), following the surface-limited replacement reduction (SLRR) method without Cu so that the surface Pt concentration was 1/3 of that for Pt/Au/Si (Yuan *et al.*, 2018); this sample is referred to as Pt/Au(111). Pt/Au(111) was loaded in the PTRF–XAFS cell (Yuan *et al.*, 2018); BCLA + TRF-XAFS was measured under 1 mm-thick solution with −0.16 $V_{Ag/AgCl}$ potential applied. Due to the limit of the beam time and low concentration, we have only measured the XANES region.

3. Results and discussion

3.1. TRF-XAFS spectroscopy with BCLA

Fig. 2 shows the L_3-edge XAFS of Pt/Au/Si under total reflection conditions in fluorescence mode without the BCLA. In the XAFS spectrum without the BCLA, strong Au $L\alpha$ X-ray fluorescence appeared above 11900 eV (the Au L_3 edge). Even under the total reflection conditions, X-rays could penetrate the bulk and excite the Au edge (Yuan *et al.*, 2017).

Fig. 3 shows the Pt L_3-edge TRF-XAFS obtained with the BCLA. We could obtain spectra under total reflection conditions where the long footprint was created on the flat Au surface. This indicated that the point focus was not necessary for the BCLA, but a parallel arrangement of the X-ray footprint and the BCLA crystal surface was necessary for data collection. We accumulated data for 60 s per point for XAFS with the BCLA (Fig. 3) and for 10 s per point for XAFS without the BCLA (Fig. 2). The Pt $L\alpha$ fluorescence X-ray signal per second was reduced to 1/160 of that without the BCLA (I_f/I_0 = 0.0024 and 0.38 at 11800 eV with and without the BCLA, respectively). This reduction in fluorescence is a tolerable level to measure the EXAFS region and occurs for two reasons. Firstly, the X-ray must go through the Si crystal in BCLA and a series of

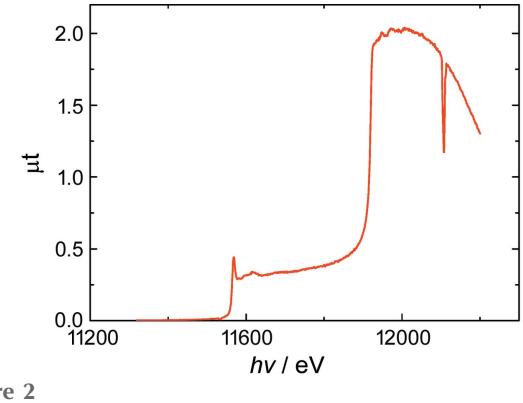

Figure 2
TRF-XAFS spectrum of Pt/Au/Si measured by SDD without the BCLA. The SDD energy window was set in the range 9.1–9.5 keV.

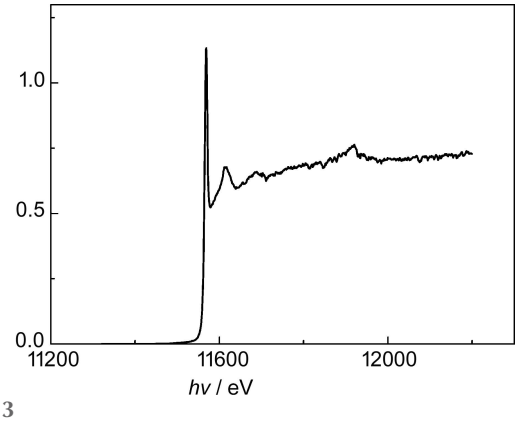

Figure 3
TRF-XAFS spectrum of Pt/Au/Si measured with the BCLA and SDD.

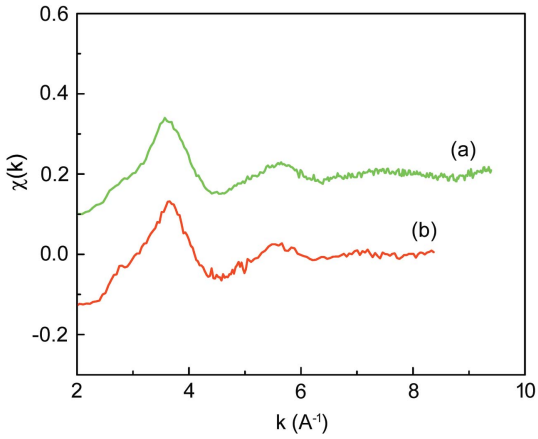

Figure 4
XAFS oscillations [$\chi(k)$] for Pt/Au/Si (*a*) with and (*b*) without BCLA.

soller slits; we estimated that the transmittance of the fluorescence X-ray was 0.2–0.3. The other reason for the reduction is the distance between the detector and the sample. As the BCLA has a focal length (5 cm in this case) and a finite width from front to back (another 8 cm), we had to put the detector 13 cm away from the sample, whereas without the BCLA we placed the SDD 2 cm away from the sample. Since the SDD has a small detector area (350 mm^2), we cannot fully use the diffracted X-rays after the BCLA. A large-area pulse-counting detector, such as PILATUS, can enhance the signal intensity after the BCLA.

We compared the X-ray intensities before and after the edges to obtain the signal-to-background (S/B) ratio. The X-ray intensity before the edge (around 11340 eV) corresponded to the background level (B), whereas that after the edge (11800 eV) corresponded to the signal (S). S/B could be estimated at 11000 with the BCLA and 140 without the BCLA. The background X-ray level was markedly reduced by the BCLA. It reduces the detection limit of TRF-XAFS. Fig. 4 shows the $\chi(k)$ data with and without the BCLA. The signal-to-noise (S/N) ratio of $\chi(k)$ was the same level with the BCLA than without. We could conclude that the combination of BCLA and TRF-XAFS was possible and we could measure the EXAFS at <1 ML concentration of Pt under grazing-incident conditions. If a high-brilliance synchrotron radiation facility is used, TRF-XAFS of <0.1 ML surface species can be detected in combination with BCLA.

3.2. Feasibility study of range-extended TRF-XAFS spectroscopy

Fig. 5 shows the results of the energy analysis of the SDD output signal before and after the Au L_3 edge without the BCLA. Pt $L\alpha$ fluorescence appeared at 9442 eV. The Pt fluorescence was hindered by strong Au $L\alpha_1$ and $L\alpha_2$, which were located at 9628 eV and 9713 eV, respectively. The strong Au fluorescence line could be removed only when we applied a small energy window of 9180–9340 eV and selected the area of the Pt $L\alpha$ emission as shown in Fig. S6.

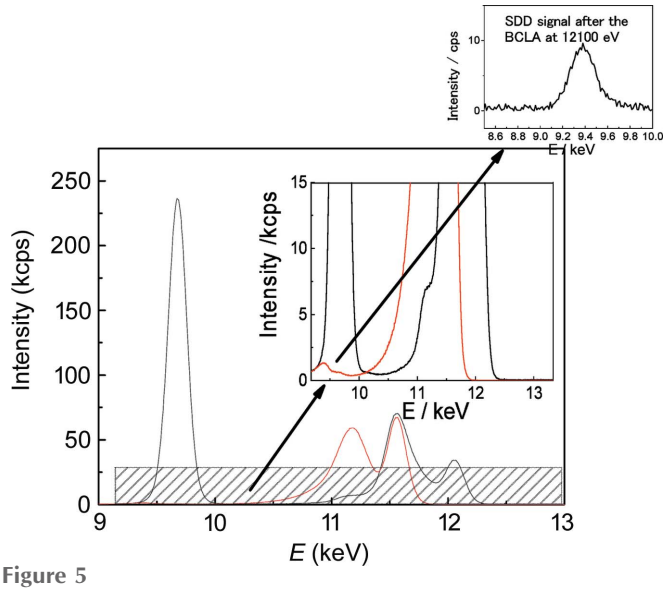

Figure 5
Spectra of X-rays detected by SDD. The red and black curves correspond to the incident X-ray energy before (11300 eV) and after (12100 eV) the Au edge, respectively; the peaks at 9442 eV and 9628 eV correspond to Pt and Au $L\alpha$, respectively.

When the BCLA was set between the sample and the SDD, Au $L\alpha$ was removed and only Pt $L\alpha$ was observed, as shown in the top insert of Fig. 5. This meant that we could perform range-extended TRF-XAFS spectroscopy using the BCLA. We previously measured the range-extended XAFS of AuPt alloy nanoparticles dispersed on an HOPG substrate in the BCLA + BI-XAFS method (Wakisaka *et al.*, 2018; Takahashi *et al.*, 2019; Feiten *et al.*, 2020). However, in the present work, a small glitch appeared at the Au L_3 edge, as shown in Fig. 3. This glitch arose from the sudden change in reflectivity at the Au L_3 edge. Under total reflection conditions, the Pt on the surface was doubly excited by the incident and the reflected X-rays so that the reflected X-rays modified the fluorescence signal due to the change of reflectivity at the Au edge. The X-ray reflectivity can be expressed as (Parratt, 1954; Heald *et al.*, 1988; Kikuta, 2011; Klockenkämper & Bohlen, 2014)

$$R = \left|\frac{E_r}{E_0}\right|^2 = \frac{h - (\theta_0/\theta_c)[2(h-1)]^{1/2}}{h + (\theta_0/\theta_c)[2(h-1)]^{1/2}}, \quad (1)$$

where θ_0 and θ_c are the incident angle (glancing angle) and critical angle, respectively; h can be expressed as

$$h = \left(\frac{\theta_0}{\theta_c}\right)^2 + \left\{\left[\left(\frac{\theta_0}{\theta_c}\right)^2 - 1\right]^2 + \left(\frac{\beta}{\delta}\right)^2\right\}^{1/2}, \quad (2)$$

$$\tilde{n} = 1 - \delta + i\beta,$$

$$\delta = \frac{n_a r_e \lambda^2}{2\pi} f_1,$$

$$\beta = \frac{\lambda}{4\pi}\mu = \frac{n_a r_e \lambda^2}{2\pi} f_2,$$

where $\tilde{n}$ and μ are the complex refraction index and absorption coefficient, respectively; f_1 and f_2 are the real and the imaginary parts of the scattering factors, and n_a and r_e are the number density and classical electron radius, respectively.

Consequently, the normalized total intensity on the surface can be expressed as

$$I_t = \left|\frac{E_r + E_0}{E_0}\right|^2 I_0 = \frac{4(\theta_0/\theta_c)^2}{h + (\theta_0/\theta_c)[2(h-1)]^{1/2}} I_0. \quad (3)$$

The fluorescence signal is proportional to the absorption coefficient of Pt,

$$I_f \propto \mu_{Pt} I_t = \mu_{Pt}\left|\frac{E_r + E_0}{E_0}\right|^2 I_0 = \frac{4(\theta_0/\theta_c)^2 \mu_{Pt}}{h + (\theta_0/\theta_c)[2(h-1)]^{1/2}} I_0. \quad (4)$$

Fig. 6 shows the I_t spectra and their incident-angle dependence derived from the tabulated f_1 and f_2 values (Gullikson, 2001; Henke *et al.*, 1993; Nelson *et al.*, 1994). The critical-angle dependence on the X-ray energy is given at the bottom of Fig. 6. The critical angle varied from 5 mrad to 7 mrad during the energy scan. When the incident angle was less than 5 mrad, where the total reflection conditions were satisfied over all energy regions, I_t showed a positive peak. At incident angles greater than the critical angle, I_t showed a negative peak. Around the critical angle (5–6 mrad), I_t changed in a complicated manner. We set the incident angle at 4–5 mrad, which was lower than the critical angle so that the spectrum gave a positive peak at the Au edge. We attempted to correct the spectra by varying the incident angle using equation (4). The terms h and θ_c in equation (4) are dependent on f_1 and f_2, where f_2 values near the edge region were obtained using μ of the Au foil which was smoothly connected to tabulated f_2 values at higher energy (12800 eV). Similarly, f_i near the edge was calculated by Kramers–Kronig transformation from μ of the Au foil near the edge and the tabulated f_2 in the extended region. Thus the obtained μ_{Pt} was then normalized. We also obtained a corrected spectrum without glitch at the Au L_3 edge as shown in Fig. 7(*a*), when we set the incident angle at θ_0 = 4.5 mrad. Fig. 7(*b*) shows the $k^3\chi(k)$ data where the glitch was removed. Fig. S5 shows the curve fitting of the data with and without the correction of the data. A Pt—O bond was assumed. Table S2 of the supporting information shows the bond distances and coordination numbers. The precision of the fitting result was slightly improved compared with that analysed before the Au absorption edge. Since the scatterer was a light element (O) and the XAFS oscillation was quickly damped, the merit was not so clear. We concluded that range-extended TRF-XAFS spectroscopy was possible using the BCLA after correction of the reflectivity by adjusting the incident angle. The merit of the range extended XAFS would be clear in the heavy-scatterer case where the XAFS oscillation lasted at the high k-region.

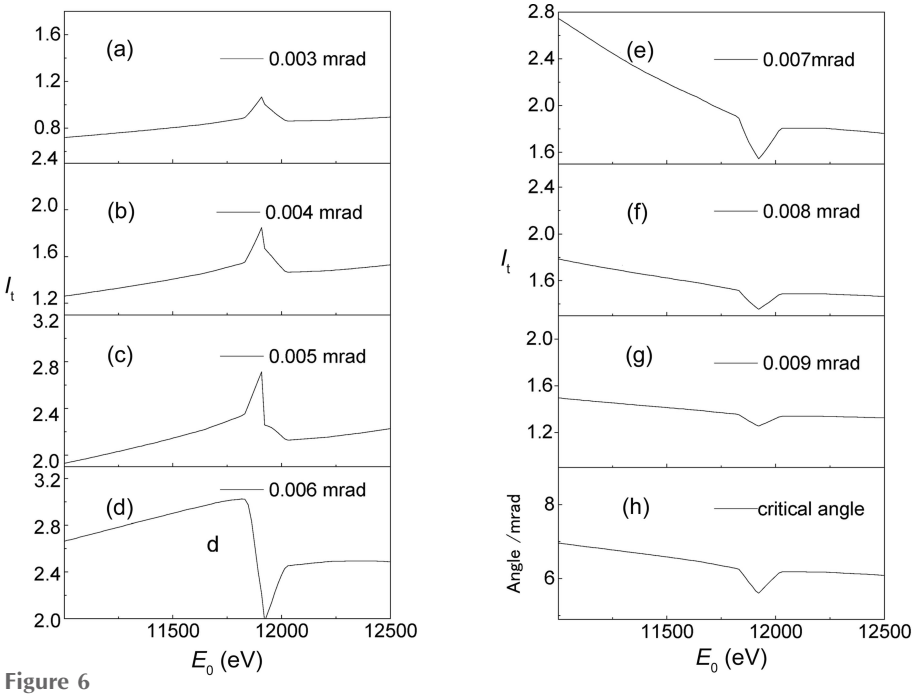

Figure 6
(*a*) Photon energy dependence of the total excitation X-ray intensity (I_t) with various critical angles (*a*)–(*g*) calculated based on the atomic scattering factors (Gullikson, 2001; Henke *et al.*, 1993; Nelson *et al.*, 1994). (*h*) Photon energy dependence of the critical angle.

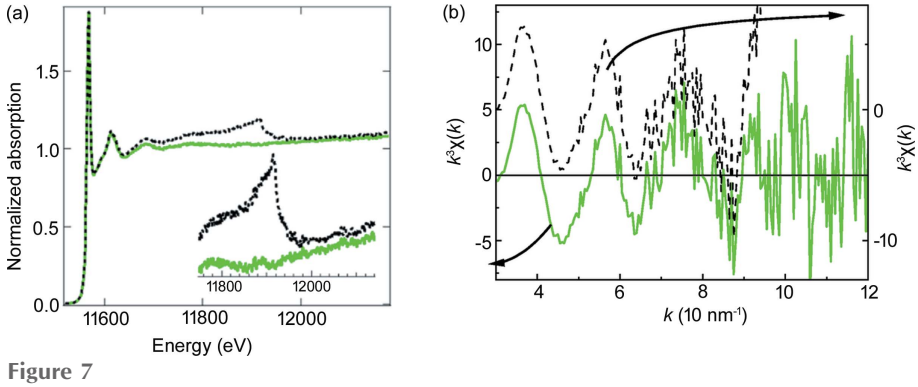

Figure 7
XAFS spectrum after absorption correction based on the experimental absorption data of (*a*) Au foil and (*b*) $k^3\chi(k)$ (black-broken and green-solid lines are for uncorrected and corrected spectra, respectively).

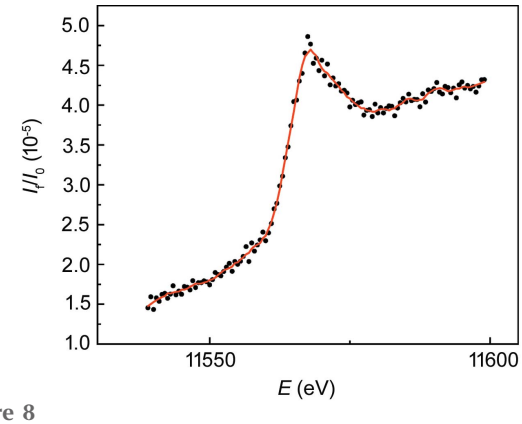

Figure 8
XANES spectra of 0.1 ML Pt on Au under −0.16 $V_{Ag/AgCl}$ potential. The electrolyte was 0.1 ML $HClO_4$ and the accumulation time was 100 s per point.

3.3. Feasibility study of BCAL + TRF-XAFS as an *in situ* surface XAFS technique

In order to study the feasibility of *in situ* BCLA + TRF-XAFS spectroscopy in the presence of a sufficiently thick solution, we carried out a preliminary measurement of BCLA + TRF-XANES on the Pt L_3 edge of Pt/Au(111) in the presence of a ∼1.0 mm-thick solution layer with the application of −0.16 $V_{Ag/AgCl}$ potential as shown in Fig. 8. Pt/Au(111) was studied to follow the structure of Pt species prepared by the spontaneous deposition process. We could obtain a cyclic voltammetry (CV) measurement with a 1 mm gap between the sample and window which was comparable with that of the same sample with a thicker solution layer as shown in Fig. S4. Thus the result indicates the possibility of *in situ* (P)TRF-XAFS under electrochemical conditions. However, the background X-rays were larger than expected from the measurement under air. This was due to the inelastic X-ray scattering from the solution overlayer that had the same energy as Pt $L\alpha$ fluorescence. This inelastic scattering from the solution determined the lower limit of the TRF-XAFS measurement. A 0.1 ML of Pt on Au in the presence of solution will be possible when using a high-brilliance synchrotron radiation source.

3.4. Comparison with other *in situ* surface XAFS techniques

There are several surface-sensitive XAFS methods to investigate highly dispersed metal nanoparticles on surfaces under reaction conditions. Total reflection XAFS spectroscopy is a way to increase surface sensitivity and fulfil *in situ* conditions (White *et al.*, 1988; Sharpe *et al.*, 1990; Lützenkirchen-Hecht *et al.*, 2003; Abe *et al.*, 2016; Keil & Lützenkirchen-Hecht, 2009; Hecht *et al.*, 1996; Uehara *et al.*, 2014). Under total reflection conditions, X-rays can only penetrate a few nanometres into the bulk. The reflectivity changes with the change in the absorption coefficient through the imaginary part of the refraction index. Kramers–Kronig transformations are used to derive the XAFS signal (Abe *et al.*, 2016; Martens & Rabe, 1980, 1981). However, it is difficult to observe XAFS for less than a few MLs of sample because of the small reflectivity change (Keil *et al.*, 2010).

Combining total reflection with fluorescence methods is more feasible to extend the lower limit (Heald *et al.*, 1984). There are two ways to detect the fluorescence signal under the total reflection condition. The first is to use the grazing incidence geometry where the incident X-ray is totally reflected. The second is to use grazing exit conditions (Meirer *et al.*, 2009) where the fluorescence X-ray from the bulk cannot be detected. Although the latter has some merits for utilization of microbeams to perform microanalysis, the signal is low and is not suitable to study surface adsorbates <1 ML thick. The former method or total reflection fluorescence XAFS have high sensitivity in a vacuum or the gas phase. Under ultrahigh-vacuum conditions, a 0.02 ML of Ni can be detected (Koike *et al.*, 2006). By combining with the polarization dependence, we can obtain the three-dimensional structure in PTRF-XAFS. In the liquid–solid interface system, PTRF-XAFS requires a less than 1 µm thick solution to reduce absorption and scattering of the solution (Tamura *et al.*, 2000; Masuda *et al.*, 2016; Yuan *et al.*, 2017, 2018). However, such a thin liquid layer hinders material diffusion and cannot follow the electrochemical process continuously.

The BCLA combined with BI-XAFS technique enables <1 ML detection of the polarization-dependent fluorescence XAFS from Pt on thin HOPG in the presence of a thick electrolyte. In the BI method, the X-rays are illuminated from the rear side of the thin HOPG with Pt species dispersed on the front side having contact with thick solution. The thin HOPG is used as the X-ray window, electrode and Pt nanoparticle support (Uehara *et al.*, 2014). This method requires a brilliant X-ray source to obtain strong X-ray intensity as a 100 µm X-ray beam size is required, as mentioned in Section 1.

In this study, we combined total reflection conditions and BCLA. The long footprint of the incident X-ray created under the grazing-incidence (total reflection) conditions can be compensated for by the parallel arrangement of the BCLA with respect to the X-ray footprint to increase the acceptance area. In spite of the loss of the fluorescence signal by the BCLA, the detection limit of (P)TRF-XAFS can be enhanced by removing the background (Fig. 3). Consequently, BCLA + (P)TRF-XAFS spectroscopy is a promising surface technique to perform *in situ* XAFS spectroscopy even in the presence of a solution thick enough for diffusion. In fact, we carried out a preliminary measurement of BCLA + PTRF-XAFS on the Pt L_3 edge of a 0.1 ML of Pt on Au(111) in the presence of a 1 mm-thick solution layer with the application of −0.16 $V_{Ag/AgCl}$ potential and we observed the corresponding XANES spectrum shown in Fig. 8.

4. Conclusions

The parallel arrangement of the BCLA to the X-ray footprint has enabled us to measure TRF-XAFS of 1 ML of Pt on an Au surface and TRF-XANES of 0.1 ML of Pt on an Au surface in the presence of solution. Although the BCLA markedly reduced the signal (1/160 compared with that without BCLA),

removal of the background X-rays by BCLA helped to enhance the S/B ratio. The range-extended TRF-XAFS can be obtained if appropriate reflectivity correction is performed. Polarization-dependent measurement is possible in principle. Thus BCLA plus a polarization-dependent TRF-XAFS (PTRF-XAFS) spectroscopy is a promising *in situ* three-dimensional surface structure analysis technique for dispersed systems even in the presence of solution.

Acknowledgements

The work was carried out under the approval of PAC (proposal Nos. 2014G040, 2016G035, 2017G628, 2019G554, and 2019G555). Part of the data was obtained under SPring-8 proposal Nos. 2018B7903, 2019A7904 and 2019A7905. The BCLA was made by the Technical Division of the Institute for Catalysis, Hokkaido University. We thank Tim Cooper, PhD, from the Edanz Group (www.edanzediting.com/ac) for editing a draft of this manuscript.

Funding information

The authors would like to acknowledge financial support from the New Energy and Industrial Technology Development Organization (NEDO) Polymer Electrolyte Fuel Cell (PEFC) project and from Grant in Aid for Scientific Research A of Japan Society for the Promotion of Science (JSPS) (proposal No. 20H00367).

References

Abe, H., Nakayama, T., Niwa, Y., Nitani, H., Kondoh, H. & Nomura, M. (2016). *Jpn. J. Appl. Phys.* **55**, 062401.
Asakura, H., Kawamura, N., Mizumaki, M., Nitta, K., Ishii, K., Hosokawa, S., Teramura, K. & Tanaka, T. (2018). *J. Anal. At. Spectrom.* **33**, 84–89.
Asakura, K. (2016). *XAFS Techniques for Catalysts, Nanomaterials and Surfaces*, edited by Y. Iwasawa, K. Asakura & M. Tada, pp. 193–206. Cham: Springer.
Asakura, K., Chun, W. J., Shirai, M., Tomishige, K. & Iwasawa, Y. (1997). *J. Phys. Chem. B*, **101**, 5549–5556.
Chun, W. J., Asakura, K. & Iwasawa, Y. (1997). *J. Phys.* **7**, 921–922.
Feiten, F. E., Takahashi, S., Sekizawa, O., Wakisaka, Y., Sakata, T., Todoroki, N., Uruga, T., Wadayama, T., Iwasawa, Y. & Asakura, K. (2020). *Phys. Chem. Chem. Phys.* **22**, 18815–18823.
Glatzel, P., Sikora, M., Smolentsev, G. & Fernández-García, M. (2009). *Catal. Today*, **145**, 294–299.
Gullikson, E. (2001). Center for X-ray Optics at the Lawrence Berkeley National Laboratory, Berkley, USA. http//:wwwcxro.lbl. gov/optical_constants/getdb2. html.
Heald, S., Chen, H. & Tranquada, J. (1988). *Phys. Rev. B*, **38**, 1016–1026.
Heald, S. M., Keller, E. & Stern, E. A. (1984). *Phys. Lett. A*, **103**, 155–158.
Hecht, D., Frahm, R. & Strehblow, H. H. (1996). *J. Phys. Chem.* **100**, 10831–10833.
Henke, B. L., Gullikson, E. M. & Davis, J. C. (1993). *At. Data Nucl. Data Tables*, **54**, 181–342.
Igarashi, N., Nitani, H., Takeichi, Y., Niwa, Y., Abe, H., Kimura, M., Mori, T., Nagatani, Y., Kosuge, T., Kamijo, A., Koyama, A., Ohta, H. & Shimizu, N. (2016). *AIP Conf. Proc.* **1741**, 040021.
Karanfil, C., Bunker, G., Newville, M., Segre, C. U. & Chapman, D. (2012). *J. Synchrotron Rad.* **19**, 375–380.
Keil, P., Frahm, R. & Lutzenkirchen-Hecht, D. (2010). *Corros. Sci.* **52**, 1305–1316.
Keil, P. & Lützenkirchen-Hecht, D. (2009). *J. Synchrotron Rad.* **16**, 443–454.
Kikuta, S. (2011). *X-ray Scattering and Synchrotron Radiation Science: Fundamentals*. University of Tokyo Press.
Klockenkämper, R. & Von Bohlen, A. (2014). *Total-reflection X-ray Fluorescence Analysis and Related Methods.* Hoboken, NJ: John Wiley.
Koike, Y., Ijima, K., Chun, W. J., Ashima, H., Yamamoto, T., Fujikawa, K., Suzuki, S., Iwasawa, Y., Nomura, M. & Asakura, K. (2006). *Chem. Phys. Lett.* **421**, 27–30.
Kropf, A., Finch, R. J., Fortner, J. A., Aase, S., Karanfil, C., Segre, C. U., Terry, J., Bunker, G. & Chapman, L. D. (2003). *Rev. Sci. Instrum.* **74**, 4696–4702.
Kujala, N. G., Karanfil, C. & Barrea, R. A. (2011). *Rev. Sci. Instrum.* **82**, 063106.
Liu, Y., Gokcen, D., Bertocci, U. & Moffat, T. P. (2012). *Science*, **338**, 1327–1330.
Liu, Y., Hangarter, C. M., Garcia, D. & Moffat, T. P. (2015). *Surf. Sci.* **631**, 141–154.
Lützenkirchen-Hecht, D., Wagemaker, M., Keil, P., van Well, A. A. & Frahm, R. (2003). *Surf. Sci.* **538**, 10–22.
Martens, G. & Rabe, P. (1980). *Phys. Status Solidi A*, **58**, 415–424.
Martens, G. & Rabe, P. (1981). *J. Phys. C Solid State Phys.* **14**, 1523–1534.
Masuda, T., Fukumitsu, H., Takakusagi, S., Chun, W.-J., Kondo, T., Asakura, K. & Uosaki, K. (2012). *Adv. Mater.* **24**, 268–272.
Masuda, T., Sun, Y., Fukumitsu, H., Uehara, H., Takakusagi, S., Chun, W., Kondo, T., Asakura, K. & Uosaki, K. (2016). *J. Phys. Chem. C*, **120**, 16200–16210.
Meirer, F., Pepponi, G., Streli, C., Wobrauschek, P. & Zoeger, N. (2009). *J. Appl. Phys.* **105**, 074906.
Nelson, C. S., Markert, T. H., Song, Y., Schattenburg, M. L., Graessle, D. E., Flanagan, K. A., Blake, R. L., Bauer, J. M. & Gullikson, E. M. (1994). *EUV, X-ray and Gamma-Ray Instrumentation for Astronomy V*, pp. 191–203. San Diego, CA: International Society for Optics and Photonics.
Parratt, L. G. (1954). *Phys. Rev.* **95**, 359–369.
Sa, J. (2014). *High-Resolution XAS/XES: Analyzing Electronic Structures of Catalysts.* Boca Raton, FL: CRC Press.
Sakayanagi, Y. (1982). *Jpn. J. Appl. Phys.* **21**, L225–L226.
Sharpe, L. R., Heineman, W. R. & Elder, R. (1990). *Chem. Rev.* **90**, 705–722.
Takahashi, S., Todoroki, N., Myochi, R., Nagao, T., Taguchi, N., Ioroi, T., Feiten, F. E., Wakisaka, Y., Asakura, K., Sekizawa, O., Sakata, T., Higashi, K., Uruga, T., Iwasawa, Y. & Wadayama, T. (2019). *J. Electroanal. Chem.* **842**, 1–7.
Tamura, K., Oyanagi, H., Kondo, T., Koinuma, M. & Uosaki, K. (2000). *J. Phys. Chem. B*, **104**, 9017–9024.
Tanizawa, Y., Shido, T., Chun, W., Asakura, K., Nomura, M. & Iwasawa, Y. (2003). *J. Phys. Chem. B*, **107**, 12917–12929.
Uehara, H., Uemura, Y., Ogawa, T., Kono, K., Ueno, R., Niwa, Y., Nitani, H., Abe, H., Takakusagi, S., Nomura, M., Iwasawa, Y. & Asakura, K. (2014). *Phys. Chem. Chem. Phys.* **16**, 13748–13754.
Wakisaka, Y., Kido, D., Uehara, H., Yuan, Q., Feiten, F. E., Mukai, S., Takakusagi, S., Uemura, Y., Yokoyama, T., Wada, T., Uo, M., Sekizawa, O., Uruga, T., Iwasawa, Y. & Asakura, K. (2019). *Chem. Rec.* **19**, 1157–1165.
Wakisaka, Y., Kido, D., Uehara, H., Yuan, Q., Takakusagi, S., Uemura, Y., Yokoyama, T., Wada, T., Uo, M., Sakata, T., Sekizawa, O., Uruga, T., Iwasawa, Y. & Asakura, K. (2018). *Catalysts*, **8**, 204.

White, J. H., Albarelli, M. J., Abruna, H. D. & Blum, L. (1988). *J. Phys. Chem.* **92**, 4432.
Yamakata, A., Uchida, T., Kubota, J. & Osawa, M. (2006). *J. Phys. Chem. B*, **110**, 6423–6427.
Yano, J., Kern, J., Irrgang, K.-D., Latimer, M. J., Bergmann, U., Glatzel, P., Pushkar, Y., Biesiadka, J., Loll, B., Sauer, K., Messinger, J., Zouni, A. & Yachandra, V. K. (2005). *Proc. Natl Acad. Sci. USA*, **102**, 12047–12052.
Yuan, Q., Takakusagi, S., Wakisaka, Y., Uemura, Y., Wada, T., Ariga, H. & Asakura, K. (2017). *Chem. Lett.* **46**, 1250–1253.
Yuan, Q., Wakisaka, Y., Uemura, Y., Wada, T., Ariga-Miwa, H., Takakusagi, S., Asakura, K. & Brankovic, S. R. (2018). *J. Phys. Chem. C*, **122**, 16664–16673.
Zhong, Z., Chapman, L. D., Bunker, B. A., Bunker, G., Fischetti, R. & Segre, C. U. (1999). *J. Synchrotron Rad.* **6**, 212–214.